dual band-reject mechanism with stubs was analyzed thoroughly. Furthermore, it can be used with other resonant or non-resonant (e.g., UWB) antenna structures in planar (e.g., rectangular, circular, elliptical) and/or volumetric configurations (e.g., rectangular, circular, elliptical, spherical, oval, cubiform), regardless of their feed mechanism.

The proposed design consists of linear sections only and is easy to replicate, fine-tune and fabricate. In addition, it is conformal, single-sided, has low gain at the rejected frequencies, low dispersion (flat group delay everywhere except at the rejected bands) that makes it useful in pulsed cognitive radio applications, while it improves the quality of UWB communication links in WLAN environments by increasing the S/N ratio at practically no additional fabrication cost.

REFERENCES

[1] Fed. Commun. Comm, "First report and order, revision of part 15 of the commission's rule regarding ultra wideband transmission systems," FCC 02-48 Apr. 22, 2002.

[2] *Part 11: Wireless LAN Medium Access Control (MAC) and Physical Layer (PHY) specifications: Physical Layer in the 5 GHz Band*, IEEE Std. 802. 11a-1999(R2003), Jun. 12, 2003.

[3] W. J. Lui, C. H. Cheng, and H. B. Zhu, "Improved frequency notched ultrawideband slot antenna using square ring resonator," *IEEE Trans. Antennas Propag.*, vol. 55, no. 9, pp. 2445–2450, 2007.

[4] Y. J. Cho, K. K. Kim, D. H. Choi, S. S. Lee, and S. O. Park, "A miniature UWB planar monopole antenna with 5 GHz band rejection filter and the time domain characteristics," *IEEE Trans. Antennas Propag.*, vol. 54, no. 5, pp. 1453–1460, 2006.

[5] T. Yang, W. A. Davis, and W. L. Stuzman, "Folded-notch dual band ultra-wideband antenna," in *Proc. IEEE APS Int. Symp*, 2005, vol. 1B, pp. 520–523.

[6] K. Bahadori and Y. Rahmat-Samii, "A miniaturized elliptic-card UWB antenna with WLAN band rejection for wireless communications," *IEEE Trans. Antennas Propag.*, vol. 55, no. 11, pp. 3326–3332, Nov. 2007.

[7] H.-Y. Lai, Z.-Y. Lei, Y.-J. Xie, G.-L. Ning, and K. Yang, "UWB antenna with dual band rejection for WLAN/WiMAX bands using CSRRs," *Progr. Electromagn. Res. Lett.*, vol. 26, pp. 69–78, Aug. 2011.

[8] C. R. Medeiros, J. R. Costa, and C. A. Fernandes, "Compact tapered slot UWB antenna with WLAN band rejection," *IEEE Antennas Wireless Propag. Lett.*, vol. 8, pp. 661–664, 2009.

[9] K. S. Ryu and A. A. Kishk, "UWB antenna with single or dual band-notches for lower WLAN band upper WLAN band," *IEEE Trans. Antennas Propag.*, vol. 57, no. 12, pp. 3942–3950, Dec. 2009.

[10] W. T. Li, X. W. Shi, and Y. Q. Hei, "Novel planar UWB monopole antenna with triple band-notched characteristics," *IEEE Antennas Wireless Propag. Lett.*, vol. 8, pp. 1094–1098, 2009.

[11] D. E. Anagnostou, H. Kim, B. Kim, S. Nikolaou, J. Papapolymerou, and M. Tentzeris, "Dual band-notched ultra-wideband antenna for 802.11a LAN environments," in *Proc. IEEE APS Int. Symp.*, Honolulu, HI, Jun. 10–15, 2007, pp. 4621–4624.

[12] R. N. Simons, *Coplanar Waveguide Circuits, Components, and Systems*. New York: Wiley, 2001, ch. 6.

[13] W.-S. Lee, D.-Z. Kim, K.-J. Kim, and J.-W. Yu, "Wideband planar monopole antennas with dual band-notched characteristics," *IEEE Trans. Microwave Tech.*, vol. 54, no. 6, pp. 2800–2806, 2006.

[14] D. M. Pozar, *Microwave Engineering*, 2nd ed. New York: Wiley, 1998.

Dual-Band Circularly Polarized Cavity-Backed Annular Slot Antenna for GPS Receiver

Wang-Ta Hsieh, Tze-Hsuan Chang, and Jean-Fu Kiang

***Abstract*—A circularly polarized (CP) cavity-backed annular slot antenna for GPS receiver is designed to operate in both the L1 and L2 bands of the Global Positioning System (GPS). The measured impedance bandwidths with VSWR less than 2 are 3.7% (1.19–1.235 GHz) and 1.2% (1.565–1.585 GHz), respectively, the measured 3 dB axial-ratio (AR) bandwidth are 0.9% (1.220–1.231 GHz) and 0.6% (1.572–1.581 GHz), respectively. A cavity is designed to render a unidirectional radiation pattern.**

***Index Terms*—Annular slot, cavity backed, circular polarization, dual-band, GPS.**

I. INTRODUCTION

Circular polarization (CP) is generally adopted in GPS and satellite communication due to Faraday rotation when signals pass through the ionosphere. GPS antennas with right-handed circular polarization (RHCP) are required to operate in both the L1 (1.575 GHz) and the L2 (1.227 GHz) bands. A circularly-polarized wave can be radiated by exciting two linearly polarized modes of the antenna, with equal amplitude, 90° phase difference, and orthogonal to each other in polarization. Such an excitation arrangement can be implemented using a single feed or dual feeds. A single-feed CP antenna is simple in structure, easy to fabricate, and requires no external feeding network [1]–[5]. With dual feeds, the input signals can be generated with a more complicated feeding structure via a hybrid or a Wilkinson power divider [6], [7].

Dual-band single-feed CP antennas have been realized in patch or slot forms [8]–[14]. In [8], four slits are engraved near the patch edges to elongate the current path, hence reducing the antenna size. Both TM_{10} and TM_{30} modes are excited to make a dual-band CP antenna, with a 1% of bandwidth within which the axial ratio (AR) is less than 3 dB. In [9], a dual-band CP patch antenna is designed by carving an asymmetric S-shaped slot to perturb the surface current, and the 3 dB AR bandwidths are 6.9% and 0.6%, respectively. In [10], a dual-band CP slot antenna is designed by attaching two deformed monopoles orthogonal to edges of a slot, and the 3 dB AR bandwidths are 9% and 11%, respectively. A dual-band CP slot antenna with dual senses has been achieved by loading two spirals at the opposite edges of a slot [11]. Patch antennas with stacked or multilayered structures have also been implemented for GPS applications in both the L1 and the L2 bands [12]–[14].

A dual-band GPS antenna is required to have, in both bands, a wide beamwidth facing the sky, a high front-to-back ratio to avoid interference from ground. In the proposed antenna, two concentric rectangular annular slots are carved on a printed circuit board (PCB) to create two

Manuscript received November 29, 2010; revised July 25, 2011; accepted September 06, 2011. Date of publication January 31, 2012; date of current version April 06, 2012. This work was sponsored by the National Science Council, Taiwan, ROC, under contract NSC 98-2221-E-002-050.

W.-T. Hsieh and J.-F. Kiang are with the Department of Electrical Engineering and the Graduate Institute of Communication Engineering, National Taiwan University, Taipei, Taiwan (e-mail: jfkiang@cc.ee.ntu.edu.tw).

T.-H. Chang is with the Foxconn, Taiwan.

Color versions of one or more of the figures in this communication are available online at http://ieeexplore.ieee.org.

Digital Object Identifier 10.1109/TAP.2012.2186229

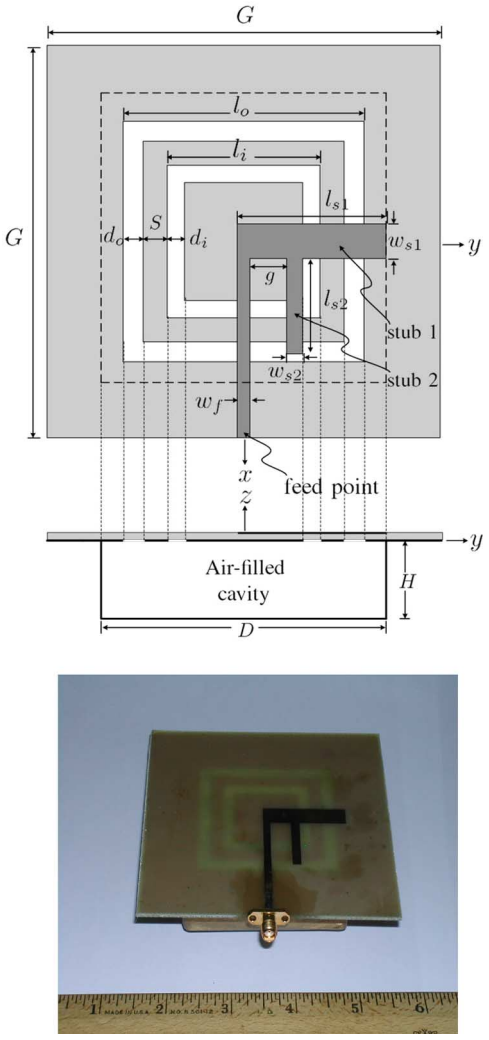

Fig. 1. Configuration and photo of the proposed antenna. Note that the drawing is not in scale.

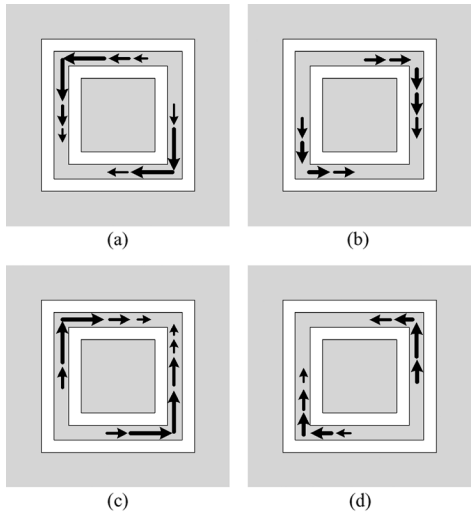

Fig. 2. Current distribution in the L2 band with period T, (a) $t = 0$, (b) $t = T/4$, (c) $t = T/2$, (d) $t = 3T/4$.

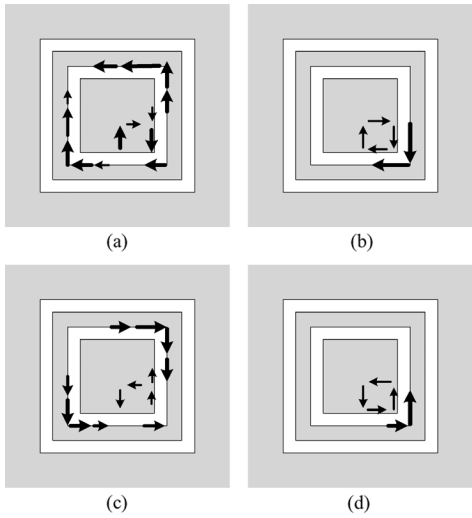

Fig. 3. Current distribution in the L1 band with period T, (a) $t = 0$, (b) $t = T/4$, (c) $t = T/2$, (d) $t = 3T/4$.

resonant frequencies at which the beamwidth is wide enough for effective reception of satellite signals. A cavity is attached to the backside of the PCB to increase the front-to-back ratio. The whole structure is compact for portable applications. An F-shape microstrip feed is laid out across these two annular slots, where two different geometrical parameters of the feed can be adjusted to match the impedance over these two bands separately, which accelerates the design process. The design considerations are described in Section II, the simulation and measurement results are presented in Section III, followed by the conclusions.

II. Design Considerations

Fig. 1 shows the configuration and photo of the proposed antenna. Two square annular slots and the microstrip feed are etched on opposite sides of an FR4 PCB with $\epsilon_r \simeq 4.4$ and 1.6 mm in thickness. A square cavity of length D and height H is soldered to the ground plane under the square annular slots. Two stubs are attached to the microstrip line with $w_f = 3$ mm to excite proper modes for CP radiation in both the L1 and the L2 bands.

The simulation results using the Ansoft HFSS indicate that two resonant modes can be excited in this slot antenna, and their resonant frequencies can be tuned to the L1 and the L2 bands, respectively, by properly adjusting various physical dimensions of the antenna. The radiation characteristics can be related either to the surface current on the conductor or to the electric field distribution over the slots. The current on the ground right beneath the microstrip line also makes slight contribution.

The surface currents concentrate near the edges of the slots, the time evolution of their distribution in both bands are displayed to help visualizing the antenna operation. Fig. 2 shows the current distribution in the L2 band, which appears to flow along the metal ring surrounded by the two slot rings. At $t = 0$, the current amplitudes at the upper left and the lower right corners rise, and their vector sum points from the upper right corner to the lower left corner. At $t = T/4$, the current amplitudes at the upper right and the lower left corners rise, and their vector sum points from the upper left corner to the lower right corner. The vector sum at $t = 0$ is orthogonal to that at $t = T/4$, typical of CP radiation. By following the movement of these vector sums with time, an RHCP radiation is expected.

Fig. 3 shows the current distribution of the antenna operating in the L1 band. The current is mainly distributed along the inner edge of the metal ring and part of the patch perimeter, in other words, around the inner slot. The vector sum of current rotates counterclockwise with

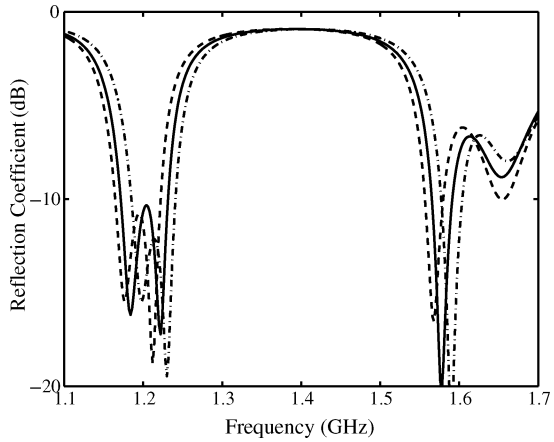

Fig. 4. Effect of outer slot width d_o on the reflection coefficient, $H = 20$, $D = 65.2, l_o = 55, l_i = 35.5, d_i = 4.5, g = 10.2, l_{s1} = 34.5, l_{s2} = 21.6$, $w_{s1} = 9, w_{s2} = 3.6$, -·-: $d_o = 4$, ——: $d_o = 4.5$, – – –: $d_o = 5$, all in unit of mm.

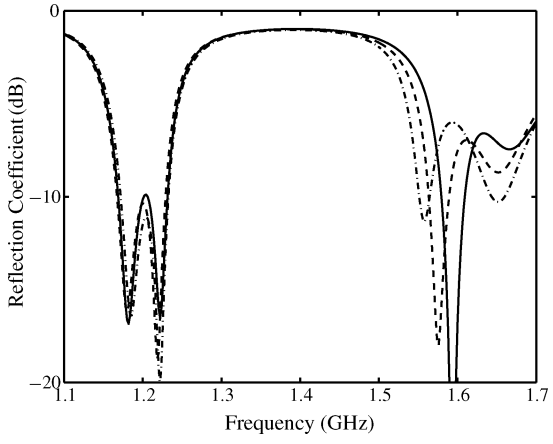

Fig. 5. Effect of second stub length l_{s2} on the reflection coefficient, $G = 100$, $H = 20, D = 65.2, l_o = 55, l_i = 35.5, d_o = 4.5, d_i = 4.5, g = 10.2$, $w_{s1} = 9, w_{s2} = 3.6, w_f = 3$, ——: $l_{s2} = 20.6$, – – –: $l_{s2} = 21.2$, -·-: $l_{s2} = 21.8$, all in unit of mm.

time, as that in the L2 band, hence an RHCP radiation is also expected. Note that the current distribution at the lower right corner is stronger than that at the upper left corner due to the proximity of the microstrip line and the stubs, underneath which a small current loop also appears. Such an asymmetry tilts the radiation pattern from the zenith by about 10°.

A. Ground Plane

Since the current mainly flows near the slots, the ground plane size has only little effect on the input impedance and the resonant frequency if the size is large enough, for example, $G \geq 80$ mm. On the other hand, the ground plane size does affect the radiation pattern, the antenna gain, and the front-to-back ratio. By simulation with HFSS, when the ground plane size G is increased from 80 to 120 mm, the antenna gain increases by 1.5 dB and the front-to-back ratio increases from 7.2 to 11.7 dB in the L2 band. In the L1 band, larger ground plane also increases the front-to-back ratio and squeezes the beamwidth. With $G = 100$ mm, the front-to-back ratio becomes higher than 10 dB.

B. Cavity

The main purpose of the cavity is to focus the radiation toward one side of the antenna. Since the cavity height H is less than $\lambda/10$ and its length D is comparable with the outer slot perimeter l_o, the cavity also interacts with the slot as part of the antenna structure. As a result, the cavity dimensions affect the input impedance and the resonant frequency of the antenna.

The effects of the cavity are analyzed by simulation using the HFSS. When the cavity height H is increased from 14 to 24 mm, the frequency with minimum axial-ratio gradually decreases, and the gain is slightly increased in both the L1 and the L2 bands. If H is less than 12 mm, the cap of the cavity becomes too close to the slot, the input impedance is strongly affected, and the radiation becomes ineffective. With all these considerations, the cavity height is chosen to be 20 mm.

As the parameter D is increased from 60 to 90 mm, the frequency with minimum axial-ratio in the L2 band gradually decreases, but that in the L1 band is hardly affected, because the cavity is closer to the outer slot and farther away from the inner slot. Note that the cavity dimensions must be taken into account when tuning the feeding structures.

C. Parameters of Slots

By simulation, when l_o or d_o increases, the resonant frequencies decrease. By increasing l_o, the stub length extending over the slot is shortened, and the input impedance is affected. Increasing d_o does not significantly affect the input impedance, but the resonant frequencies are shift downward, as shown in Fig. 4. On the other hand, it is found that l_i obviously affects the input impedance and the resonant frequency in both the L1 and the L2 bands. When l_i is increased from 30 to 32 mm, the resonant frequencies shift downward from 1.59 to 1.56 GHz and from 1.23 to 1.21 GHz, respectively. Note that d_i has little effect when it varies from 4 to 5.5 mm. Based on these observations, one may first adjust l_o and l_i to reach the required resonant frequencies while keeping the input impedance well matched, then fine tune the resonant frequencies by adjusting d_o.

D. Parameters of Feeding Structure

The input impedance can be optimized by tuning the geometrical parameters of the feeding structure, $l_{s1}, l_{s2}, w_{s1}, w_{s2}$, and g. Since the first stub passes over both the inner and outer slots, its width w_{s1} and length l_{s1} affect both the L1 and the L2 bands. When l_{s1} is increased, the resonant frequency of the L2 band decreases, and its impedance bandwidth is also increased. If l_{s1} is further increased, the L2 band will split into two bands. In additional, longer l_{s1} renders better impedance matching in the L1 band.

The second stub passes over the inner slot and extends partially over the outer slot. The resonant frequency and impedance in the L1 band are obviously affected by l_{s2}. When l_{s2} is decreased from 21.8 to 20.8 mm, the L1 resonant frequency increases from 1.56 to 1.59 GHz, and better input impedance matching is obtained, while the L2 band remains unaffected, as shown in Fig. 5. This means that usable CP radiation in the L1 band can be achieved by adjusting l_{s2}, without affecting the performance in the L2 band. In this design, we choose $l_{s2} = 21.8$ mm to achieve good impedance matching and CP radiation.

The stub widths w_{s1} and w_{s2} affect the coupling between the feeding structure and the slots. When w_{s1} is increased from 8 to 10 mm, impedance matching is improved in the L2 band. On the other hand, when the second stub width w_{s2} is decreased, impedance matching is improved in the L1 band. The stub separation g also affects the impedance matching. It is found that increasing g will shift the L1 band upward, and $g = 8.4$ mm is an optimum value to match the input impedance in both the L1 and the L2 bands.

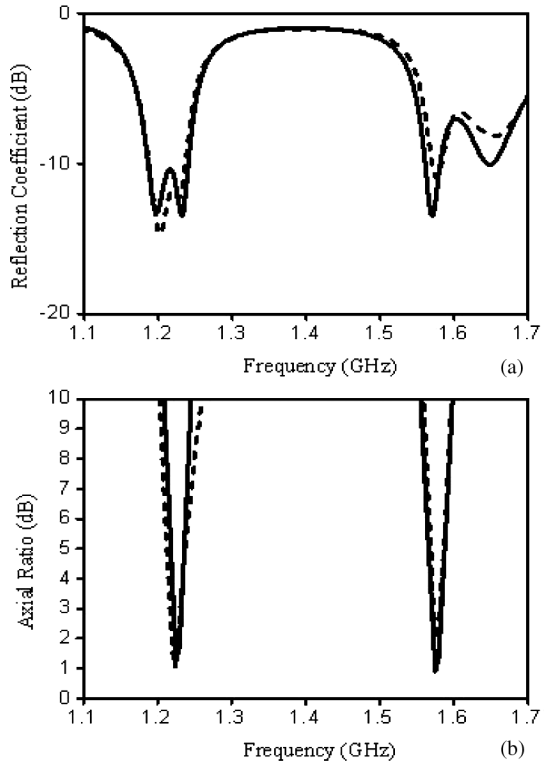

Fig. 6. Measured (——) and simulated – – – (a) reflection coefficient and (b) axial ratio, $D = 65.2$, $l_o = 55.2$, $l_i = 35$, $d_o = 4.6$, $d_i = 4$, $l_{s1} = 34.6$, $l_{s2} = 21.2$, $w_{s1} = 8$, $w_{s2} = 3.6$, $g = 8.4$, all in unit of mm.

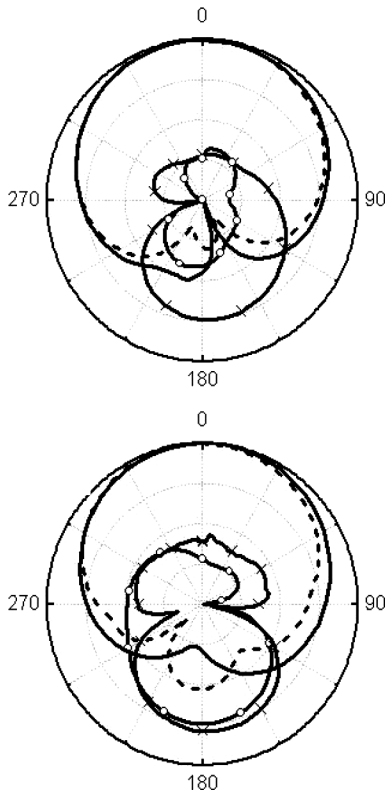

Fig. 7. Radiation patterns at 1.227 GHz: (a) $x-z$ plane, (b) $y-z$ plane, ——: measured RHCP, – – –: simulated RHCP, – ∘ –: measured LHCP, – × –: simulated LHCP, 10 dB per division on radials, all parameters are the same as in Fig. 6.

In summary, the resonant frequencies are mainly determined by the slot dimensions L_o and L_i, and are slightly affected by the geometries of the feed and the cavity. In practice, first choose proper L_o and L_i to acquire the desired bands, then adjust the geometry of the F-shaped microstrip feed to achieve impedance matching at both bands. Finally, use simulation tools like HFSS to fine-tune relevant geometrical parameters to better match the impedance at both bands. It is observed that L_o affects both modes while l_{s1} only affects the second mode. Hence, one can tune the ratio of these two resonant frequencies by adjusting l_{s1}. The size of ground plane only affects the radiation pattern, and can be used to further increase the front-to-back ratio.

III. Results and Discussions

The proposed CP antenna can be designed by adjusting the dimensions of the inner and the outer slots to roughly determine the operating frequencies, then parameters of the feeding structure can be fine tuned to achieve the required frequency bands with good impedance matching. Fig. 6 shows the measured and simulated reflection coefficient and axial ratio, respectively. The measured 10 dB impedance bandwidths are 3.7% (1.19–1.235 GHz) and 1.2% (1.565–1.585 GHz), while the 3-dB AR bandwidths are 0.9% (1.220–1.231 GHz) and 0.6% (1.572–1.581 GHz), respectively. The measurement results match reasonably well with the simulation results. The measured axial ratios at 1.227 GHz and 1.575 GHz are 1.39 dB and 2 dB, respectively.

Figs. 7 and 8 show the measured radiation patterns at 1.227 GHz and 1.575 GHz, respectively. The radiation efficiencies are about 86.5% and 80.7% in the L1 and the L2 band, respectively. The 3 dB AR beamwidth is about 100° in both the L1 and the L2 bands. The main beam in the L1 band is steered away from the zenith because of the asymmetric current distribution around the corners of the inner slot, as discussed in Section II. The beamwidth in any vertical cross section is about 100°, suitable for receiving GPS signals.

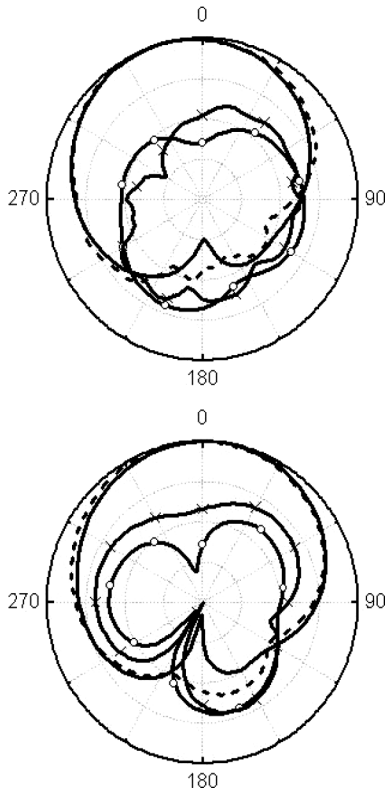

Fig. 8. Radiation patterns at 1.575 GHz: (a) $x-z$ plane, (b) $y-z$ plane, ——: measured RHCP, – – –: simulated RHCP, – ∘ –: measured LHCP, – × –: simulated LHCP, 10 dB per division on radials, all parameters are the same as in Fig. 6.

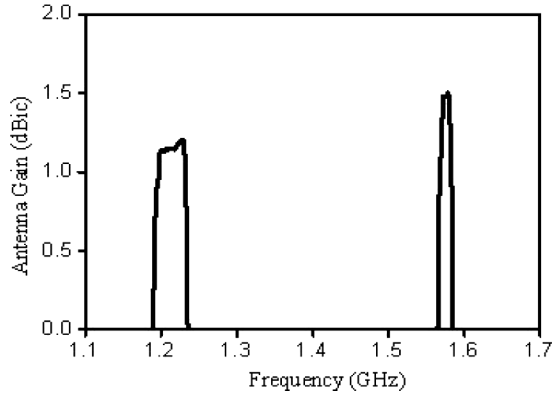

Fig. 9. Measured antenna gain, other parameters are the same as in Fig. 6.

Fig. 9 shows the measured antenna gain of the proposed antenna, which exceeds 1.45 dBic in the L1 band and exceeds 1.1 dBic in the L2 band. The simulated gain curve has the same shape as the measured one, except that the gains are 2.95 dBic and 1.5 dBic in the L1 and L2 bands, respectively.

In practice, the GPS module with RF and signal processing circuits can be attached to the PCB behind the ground plane, close yet outside the cavity wall, and is connected to the feed point as shown in Fig. 1 through a via. In this manner, the antenna properties are unaffected, and the circuits are also shielded by the ground plane from radiation.

IV. Conclusions

A dual-band circularly polarized (CP) cavity-backed annular slot antenna with a single feed is designed and measured. This antenna covers both the L1 and L2 bands of GPS. A cavity back is designed to enhance the front-to-back ratio of the radiation patterns.

References

[1] J. S. Row and S. W. Wu, "Circularly-polarized wide slot antenna loaded with a parasitic patch," *IEEE Trans. Antennas Propag.*, vol. 56, no. 9, pp. 2826–2832, Sep. 2008.

[2] J. S. Row, "The design of a square-ring slot antenna for circular polarization," *IEEE Trans. Antennas Propag.*, vol. 53, no. 6, pp. 1967–1972, June 2005.

[3] H. M. Chen, Y. K. Wang, Y. F. Ling, C. Y. Lin, and S. C. Pan, "Microstrip-fed circularly polarized square-ring patch antenna for GPS applications," *IEEE Trans. Antennas Propag.*, vol. 57, no. 4, pp. 1264–1267, Apr. 2009.

[4] K. F. Hung and Y. C. Lin, "Novel broadband circularly polarized cavity-backed aperture antenna with traveling wave excitation," *IEEE Trans. Antennas Propag.*, vol. 58, no. 1, pp. 35–42, Jan. 2010.

[5] K. F. Tong and T. P. Wong, "Circularly polarized U-slot antenna," *IEEE Trans. Antennas Propag.*, vol. 55, no. 8, pp. 2382–2385, Aug. 2007.

[6] Y. X. Guo, L. Bian, and X. Q. Shi, "Broadband circularly polarized annular-ring microstrip antenna," *IEEE Trans. Antennas Propag.*, vol. 57, no. 8, pp. 2474–2477, Aug. 2009.

[7] K. M. Mak and K. M. Luk, "A circularly polarized antenna with wide axial ratio beamwidth," *IEEE Trans. Antennas Propag.*, vol. 57, no. 10, pp. 3309–3312, Oct. 2009.

[8] K.-P. Yang and K.-L. Wong, "Dual-band circularly-polarized square microstrip antenna," *IEEE Trans. Antennas Propag.*, vol. 49, no. 3, pp. 377–382, Mar. 2001.

[9] Nasimuddin, Z. N. Chen, and X. Qing, "Dual-band circularly polarized S-shaped slotted patch antenna with a small frequency-ratio," *IEEE Trans. Antennas Propag.*, vol. 58, no. 6, pp. 2112–2115, Jun. 2010.

[10] C.-H. Chen and E. K. N. Yung, "Dual-band circularly-polarized CPW-fed slot antenna with a small frequency ratio and wide bandwidths," *IEEE Trans. Antennas Propag.*, vol. 59, no. 4, pp. 1379–1384, Apr. 2011.

[11] C.-H. Chen and E. K. N. Yung, "Dual-band dual-sense circularly-polarized CPW-fed slot antenna with two spiral slots loaded," *IEEE Trans. Antennas Propag.*, vol. 57, no. 6, pp. 1829–1834, Jun. 2009.

[12] D. M. Pozar and S. M. Duffy, "A dual-band circularly polarized aperture-coupled stacked microstrip antenna for global positioning satellite," *IEEE Trans. Antennas Propag.*, vol. 45, no. 11, pp. 1618–1625, Nov. 1997.

[13] Y. F. Wang, J. J. Feng, J. B. Cui, and X. L. Yang, "A dual-band circularly polarized stacked microstrip antenna with single-fed for GPS applications," in *Proc. IEEE Int. Symp. Antennas Propag.*, 2008, pp. 108–110.

[14] E. G. Doust, M. Clenet, V. Hemmati, and J. Wight, "An aperture-coupled circularly polarized stacked microstrip antenna for GPS frequency bands L1, L2, and L5," presented at the IEEE Int. Symp. Antennas Propag., 2008.

Design of Small Antennas for Mobile Handsets Using Magneto-Dielectric Material

Jungyub Lee, Jeongkyu Heo, Joonghee Lee, and Youngho Han

***Abstract*—This communication presents practical implementations of small antennas using magneto-dielectric (MD) materials. We first describe the manufacturing process of MD materials with a low-loss property ($\tan \delta_m < 0.1$) up to 2 GHz. With this MD material as a substrate, miniaturized handset antennas are developed and the radiation performances are compared with the dielectric substrate antenna. The measured results show that the required volume of MD chip antenna is minimized to $25\ \text{mm} \times 5\ \text{mm} \times 3\ \text{mm}$ at cellular frequency and the bandwidth is better compared to dielectric chip antennas. In addition, MD loaded antenna is designed to improve the performance of conventional antennas on the plastic carriers.**

***Index Terms*—Antennas, ferrites, loaded antennas, magnetic materials, mobile antennas.**

I. Introduction

The rapid evolution of the mobile environment demands a handheld device to support a variety of communication networks. To fulfill such a requirement, a multi-band antenna is necessary. However, the space allowed for the antenna is kept down due to the size increase of the other electronic components (e.g., battery) and the consumer preference on thinner and light platforms. This creates a technical challenge for antenna engineers to design a wideband antenna with a small form factor.

There has been a lot of research on electrically small antennas, some of them have focused on optimizing conductive parts of the antenna. Various electrical elements, such as meander lines, capacitive loads, and parasitic stubs, have been used in conjunction with the main antenna pattern to lower the resonant frequency and to widen

Manuscript received July 13, 2011; revised September 05, 2011; accepted October 26, 2011. Date of publication February 03, 2012; date of current version April 06, 2012.

J. Lee, J. Heo, and J. Lee are with the Samsung Electronics Co., Ltd., Suwon, Korea (e-mail: jungyub.lee@samsung.com).

Y. Han is with the Department of Advanced Material Engineering, Sungkyunkwan University, Suwon, Korea.

Color versions of one or more of the figures in this communication are available online at http://ieeexplore.ieee.org.

Digital Object Identifier 10.1109/TAP.2012.2186271